 doi:10.20944/preprints202105.0159.v1

Oscillatory Reversible Osmotic Growth of Sessile Saline Droplets on the Floating Polydimethylsiloxane Membrane

Pritam Kumar Roy[a], Shraga Shoval[b], Leonid A. Dombrovsky[c,d], Edward Bormashenko[a*]

[*a] *Chemical Engineering Department, Faculty of Engineering, Ariel University, P.O.B. 3, 407000, Ariel, Israel.* edward@ariel.ac.il

[b] *Department of Industrial Engineering and Management, Faculty of Engineering, Ariel University, P.O.B. 3, 407000, Ariel, Israel.*

[c] *X-BIO Institute, University of Tyumen, 6 Volodarskogo St, Tyumen, 625003, Russia.*

[d] *Heat Transfer Department, Joint Institute for High Temperatures, 17A Krasnokazarmennaya St, Moscow, 111116, Russia.*

Correspondence: edward@ariel.ac.il

*Author to whom correspondence should be addressed.

Abstract

We report cyclic growth/retraction phenomena observed for saline droplets placed on the cured PDMS membrane with the thickness of 7.8±0.1 μm floating on pure water surface. Osmotic mass transport across the micro-scaled floating PDMS membrane provided the growth of the sessile saline droplets followed by evaporation of the saline droplets. The observed growth/retraction cycle was reversible. The model of the osmotic mass transfer across the cured PDMS membrane is suggested. The model explains semi-quantitatively the time evolution of a droplet.

Keywords*:* osmotic membrane; Polydimethylsiloxane; saline droplet; mass transport; evaporation; reversible cycle.

1. Introduction

Polydimethylsiloxane (PDMS) membranes are broadly used for the manufacturing of microfluidic devices [1], separation of organics from water [2-3], gas separation [4-9] and removing aldehydes from the reactants [10]. Osmotic mass transport across PDMS-

Preprints (www.preprints.org) | NOT PEER-REVIEWED | Posted: 10 May 2021 doi:10.20944/preprints202105.0159.v1

based liquid layers was already implemented for the controlled crystallization of proteins [11-12]. In the present research, we demonstrate osmotic mass transport between the saline water encapsulated within a composite liquid marble coated with liquid PDMS and the supporting water [13]. PDMS membranes may be manufactured by dip- or spin-coating [14] and also by 3D printing [15]. The cured PDMS osmotic membranes may be manufactured by drop-casting on the water/vapor interface. Moreover, osmotic PDMS membranes enable completely reversible growth/retraction oscillations of sessile saline droplets deposited on the floating PDMS membranes. The observed oscillations of the droplets are explained by the osmotic mass transport and evaporation cycles described below.

2. Materials and Methods

Materials

The following materials were used in the recent experiment: polystyrene Petridis ($55\ mm \times 16\ mm$); poly (dimethylsiloxane) (PDMS) Sylgard 184, supplied by Dow Corning, USA (with the following characteristics: molecular weight 207.4 g/mol, viscosity 5.5 Pa× s, surface tension 20.4 mN/m); deionized water (DI) from Millipore SAS (France) (with the following characteristics: specific resistivity $\hat{\rho} = 18.2\text{M}\Omega \times \text{cm}$ at 25 °C, surface tension γ = 72.9 mN/m; viscosity $\eta = 8.9 \times 10^{-4}\text{Pa}\times\text{ s}$); Sodium chloride (NaCl) was supplied by Melach Haaretz Ltd., Israel. 5 mL droplets of the saturated aqueous NaCl solution (25.9% w/w) were used in the experiment. The thickness of PDMS membrane was established by weighting as 7.8±0.1 μm.

Methods

The floating PDMS membrane was prepared as depicted in **Figure 1** by pouring of a mixture containing liquid PDMS and a curing agent on the distilled water/vapor interface (the details of the procedure are addressed in the Materials and Methods Section). Afterwards a 5 μL saline droplet was placed on the PDMS membrane, floating within the closed vessel (chamber), as shown in **Figure 2**.

A mixture of PDMS and the crosslinker (Sylgard 184 silicone elastomer curing agent) was prepared with a weight ratio of 10 : 1. After that, a polystyrene Petridis was taken and half-filled with DI water. Then 10 μL of the PDMS mixture was gently deposited on top of the surface and kept it at room temperature for curing. After the complete

Preprints (www.preprints.org) | NOT PEER-REVIEWED | Posted: 10 May 2021 doi:10.20944/preprints202105.0159.v1

curing of PDMS mixture at room temperature (the curing time was 48 hours), a 5 µL saline droplet (saturated solution) was deposited, and simultaneously, a video was captured to observe the time variation of the droplet diameter. The preparation method is schematically shown in **Figure 1**. The contact angle of the saline droplet on the PDMS membrane is $\theta = 87° \pm 2°$.

A digital microscope BW1008-500X and Ramé-Hart advanced goniometer model 500-F1 were used to capture images and movies of the saline droplet. The experiments were carried out at an ambient air temperature of $t = 25°C$. The relative humidity of air was equal to RH = 44±2%.

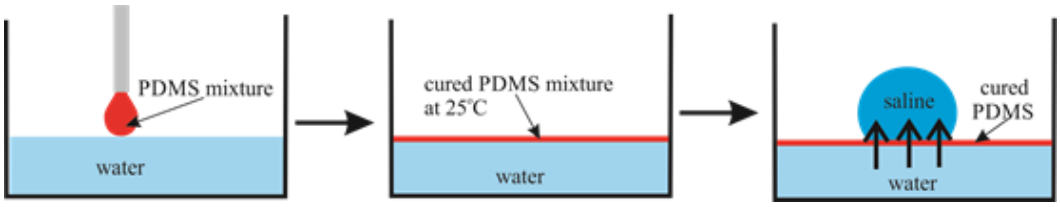

Figure 1: Schematic representation of the PDMS membrane preparation method.

3. Results and discussion

The floating PDMS membrane was prepared as depicted in **Figure 1** by pouring of a mixture containing liquid PDMS and a curing agent on the distilled water/vapor interface and as described in detail in the Materials and Methods Section). Afterwards 5-15 µL saline droplets were placed on the PDMS membrane, floating within the closed vessel (chamber), as shown in **Figure 2**. Osmotic mass transport across the PDMS membrane gave rise to the increase in the volume of the droplet, accompanied by advancing motion of the triple (three-phase) line, as depicted in **Figure 2** (diffusion of water through thin oil layers was reported recently in ref. 16). We performed two series of experiments with (i) long-range and (ii) short-range cycles of the osmotic growth/evaporation of droplets as described below. Time evolution of the droplet contact radius *r(t)* and the apparent contact angle $\theta_{app}(t)$ shown in **Figure 3** were registered with the goniometer.

Preprints (www.preprints.org) | NOT PEER-REVIEWED | Posted: 10 May 2021 doi:10.20944/preprints202105.0159.v1

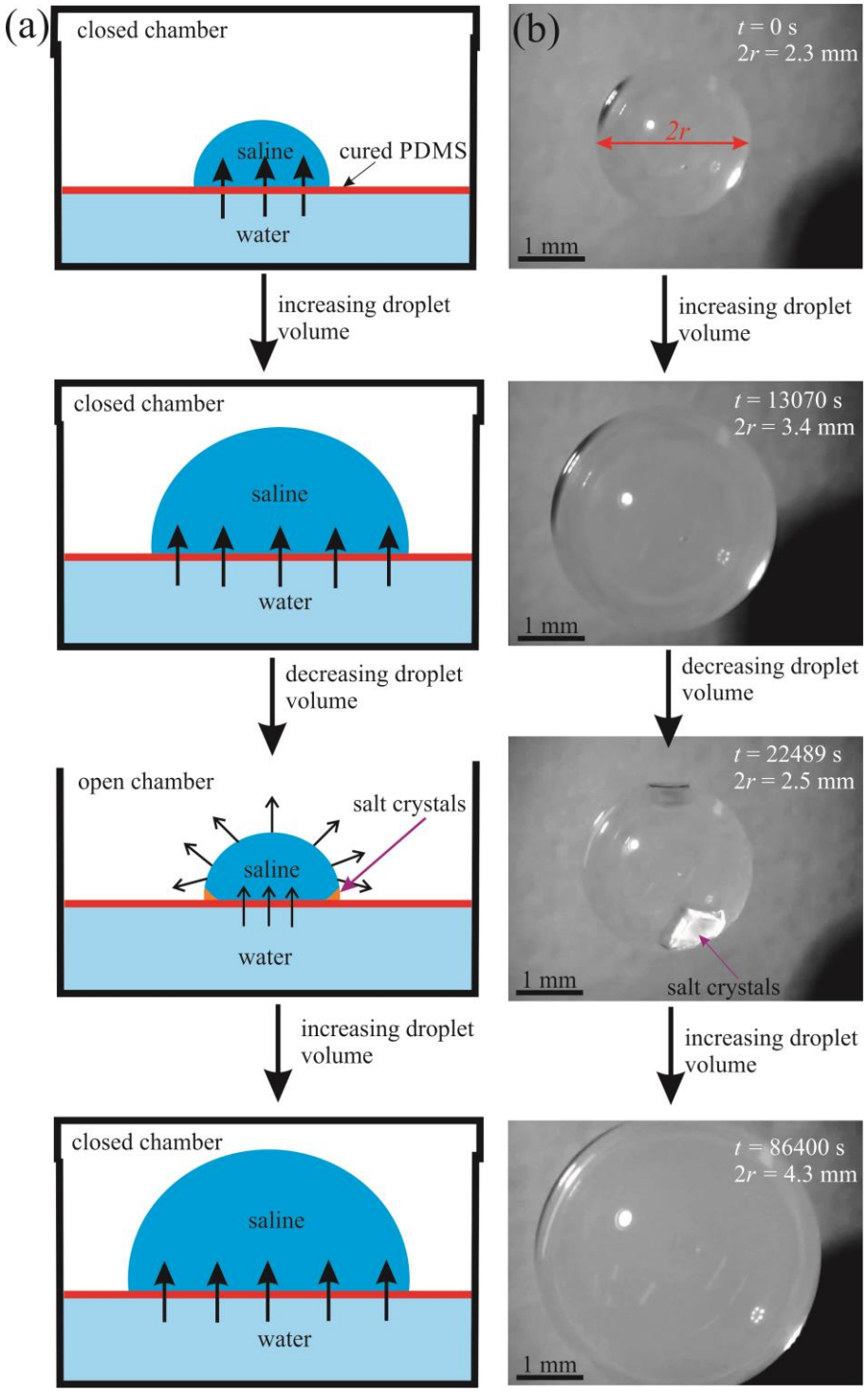

Figure 2. Growth and decay of a 5 µL saline droplet on a floating PDMS membrane due to the osmosis and evaporation; (a) schematic and (b) images.

Preprints (www.preprints.org) | NOT PEER-REVIEWED | Posted: 10 May 2021 doi:10.20944/preprints202105.0159.v1

i) At the long-time experiments, the stage of growth continued for $\tau_{gr} = 13070 \pm 0.2\ s$. During this time the droplet volume increased from 5 μL to 30 μL. Afterwards the chamber was opened, as shown in **Figure 2** and **Movie S1**, and the droplet was evaporated during $\tau_r = 11419 \pm 0.2s$. Increasing the evaporation time scale gives rise to the formation of the NaCl crystals in the vicinity of the triple line as shown in **Figure 2**. At this stage, the volume of the droplet was decreased, and the triple line retracted. We performed $n = 2$ cycles of the long-time osmotic growth/evaporation of a droplet, and observed that the process is reversible.

ii) Short-time growth/evaporation (retraction) experiments are illustrated in **Figure 4** and **Movie S2**, depicting the cyclic change in the volume V and contact diameter D of the droplet. In these experiments, the time scales were $\tau_{gr} = \tau_r = 3600 \pm 0.2\ s$; $n = 5$, of reversible growth/evaporation cycles were performed.

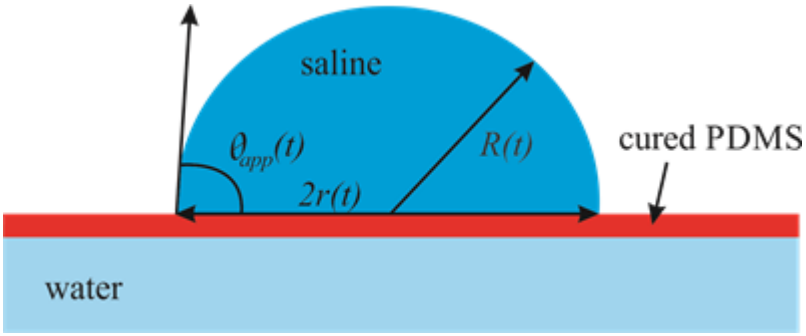

Figure 3. Geometrical parameters of saline drop placed on the floating PDMS membrane are depicted. *R(t)* is the current radius of the drop; *r(t)* is the current radius of the contact area and $\theta_{app}(t)$ is the apparent contact angle of the drop.

The initial volume of the droplets in these experiments was confined within the range of $5\mu L \leq V \leq 15\mu L$. The final volumes of the droplets were $7\mu L \leq V \leq 19\mu L$. The change in volume and contact diameter of a droplet was accompanied with a change in the apparent contact angle, illustrated in **Figure 5**. The range of the apparent contact angles registered during the osmotic growth/retraction cycles was established as $65° \pm 2° < \theta_{app} < 87° \pm 2°$. This change in the apparent contact angle is reasonably attributed to the phenomenon of the contact angle hysteresis [17-23]. In our experiments, this hysteresis is strengthened by the pinning of the triple line arising from the coffee-stain effect inevitable under evaporation of saline droplets [23-26]. The

Preprints (www.preprints.org) | NOT PEER-REVIEWED | Posted: 10 May 2021 doi:10.20944/preprints202105.0159.v1

coffee-stain effect is evidenced by formation of NaCl crystals close to the triple line, as depicted in **Figure 2**.

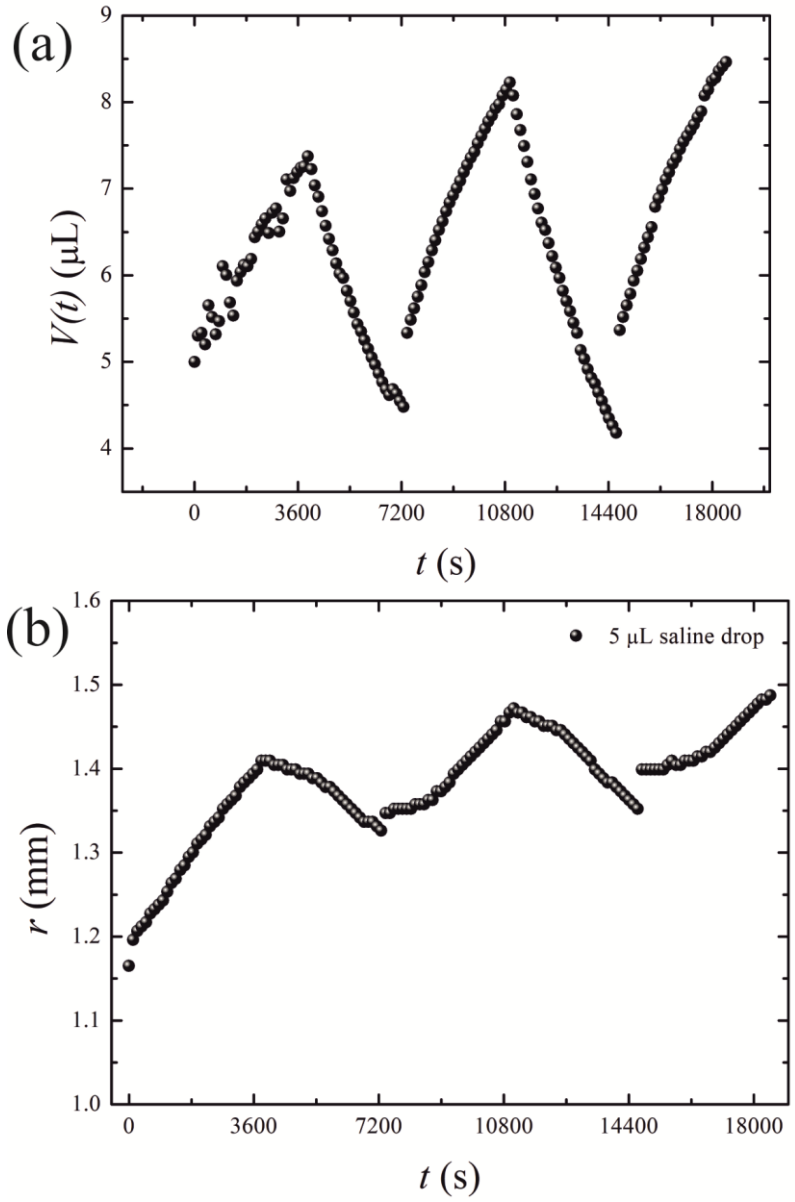

Figure 4. Oscillatory behavior of the droplets exposed to the osmotic mass transport/evaporation cycles is depicted. (a) time evolution of the drop volume *V(t)* is shown b) the time dependence of the contact radius *r* is depicted.

Preprints (www.preprints.org) | NOT PEER-REVIEWED | Posted: 10 May 2021 doi:10.20944/preprints202105.0159.v1

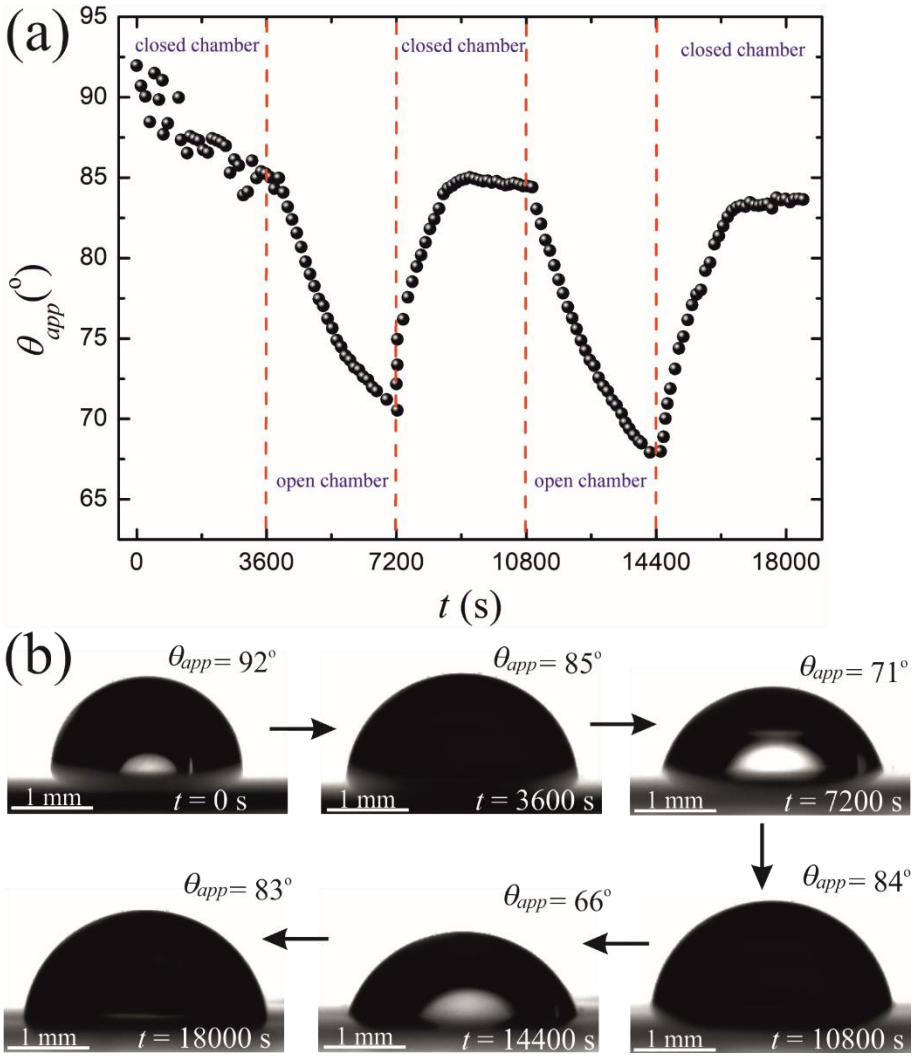

Figure 5. (a) Time evolution of the apparent contact angle $\theta(t)$ is depicted.

(b) Sequence of images illustrating the side view of the time evolution of the droplet placed on the PDMS membrane is shown.

Address now the stage of the osmotic growth of the droplets in more details as illustrated in **Figure 6**. Consider an approximate model of the osmotic growth of water droplet observed in recent experiments. In contrast to spherical small liquid marbles, addressed recently in ref. 13, the water droplet is almost hemispherical. This leads to the following mass balance equations for the time evolution of the radius of the droplet:

$$\tau_{osm}\bar{R}^3\dot{\bar{R}} = 1 \ , \tag{1}$$

$$\tau_{osm} = 2\rho_{\mathrm{w}}R_0/\psi_{osm}, \tag{2}$$

where $\bar{R}(t) = R(t)/R_0$ is the dimensionless current radius of the droplet, R_0 is the initial radius of the droplet, ρ_{w} is the density of water, ψ_{osm} is the unknown osmotic

Preprints (www.preprints.org) | NOT PEER-REVIEWED | Posted: 10 May 2021 doi:10.20944/preprints202105.0159.v1

parameter of the membrane describing the osmotic mass transport flow across the membrane, with the dimensions of $[\psi_{osm}] = \frac{kg}{m^2 s}$, and τ_{osm} is the characteristic time of the process.

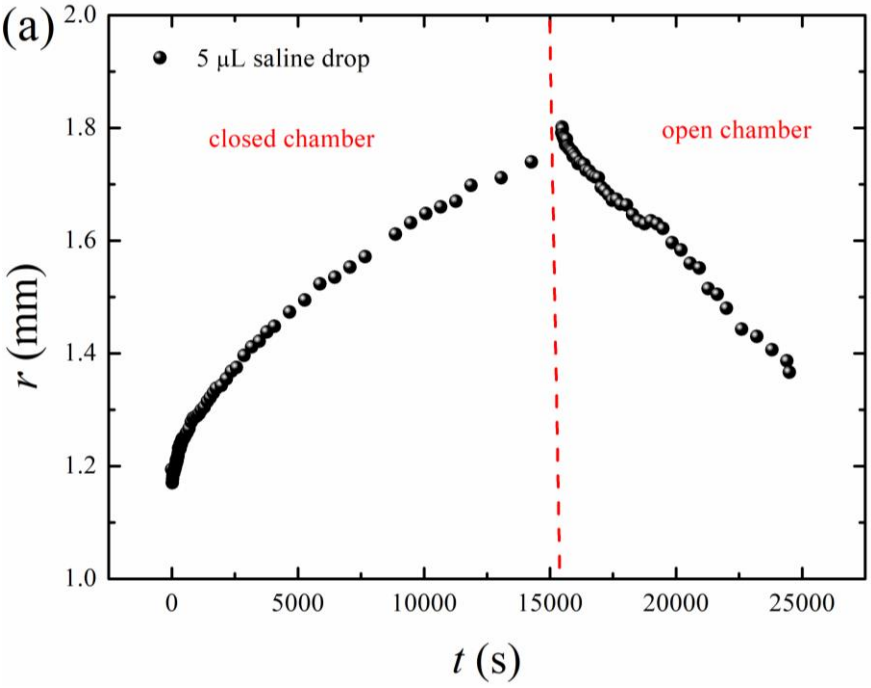

Figure 6. Growth and decay of a 5 µL saline drop on a floating PDMS membrane due osmosis and evaporation.

Radius of the studied droplets was smaller than the capillary length, which is $l_{ca} = 2.71\,mm$ for water droplets [23] and the apparent contact angles were close to $\frac{\pi}{2}$; thus, the shape of the droplets is taken as semi-spherical. The obvious initial condition for the droplet radius is given by Eq. 2:

$$\bar{R}(0) = 1 \tag{3}$$

In contrast to osmotic growth of marbles, it is reasonable to assume that the parameters ψ_{osm} and τ_{osm} are constant (independent of time) because there are no changes in the thickness and structure of the cured PDMS membrane during the mass transport. The analytical solution to the Cauchy problem, defined by Eqs. 1-3 is supplied by Eq. 4:

$$\bar{R} = \sqrt[4]{1 + \bar{t}}, \tag{4}$$

where $\bar{t} = t/\tau_{osm}$ is the dimensionless time of the osmotic evolution of the droplet.

At the beginning of the process (at $\bar{t} \ll 1$), Eq 3 is approximated as:

Preprints (www.preprints.org) | NOT PEER-REVIEWED | Posted: 10 May 2021 doi:10.20944/preprints202105.0159.v1

$$\bar{R} = 1 + 0.25\bar{t} \quad (4)$$

The linear approximation describes satisfactorily the initial stage of the osmotic growth of droplets, which is well fitted by the linear equation $\bar{R} = 1 + 0.25\bar{t} = 1 + +0.25\frac{t}{\tau_{osm}}$, as shown in **Figure 7**. The characteristic time scale τ_{osm} is slightly dependent on the initial volume of a droplet, and it was established from the experimental data as $\tau_{osm} = 4875 - 5060\ s$ for the droplets with an initial volume within 5-15 μl. The phenomenological parameter $\psi_{\text{osm}} = \frac{2\rho_w R_0}{\tau_{osm}}$ is confined (for the same initial volumes of droplets) within the range of $\psi_{osm} = 0.5 - 0.7\frac{g}{m^2 s}$. Thus, we conclude that the phenomenological parameters appearing in the constituting equations describing the osmotic mass transfer are only slightly dependent on volume of droplets.

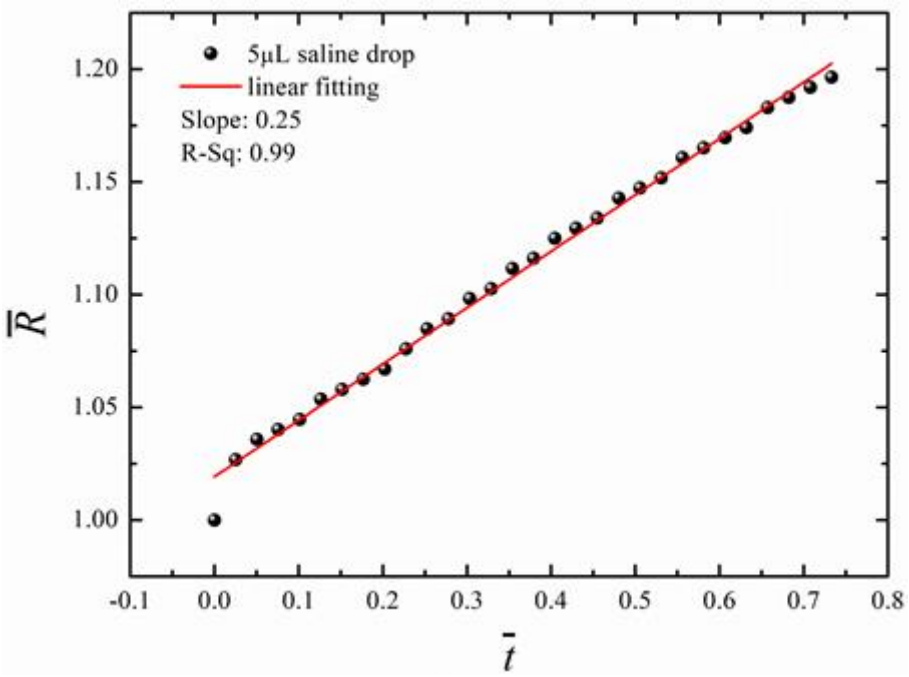

Figure 7. Experimental curve describing the osmotic evolution of a droplet during the "short time" growth, the red solid line demonstrates the best linear fitting of the experimental data depicted with black circles with the equation $\bar{R} = 1 + 0.25\bar{t} = 1 + 0.25\frac{t}{\tau_{osm}}$. $\bar{R} = \frac{R}{R_0}$ and $\bar{t} = \frac{t}{\tau_{osm}}$, where R_0 = 1.2 mm and $\tau_{osm} = 4875 \pm 10\ s$.

The linear approximation fits satisfactorily the experimental data, as it recognized from **Figure 7**, and, thus, it justifies the simplified mass transport model, described by Eqs. 1-2, implying the assumptions: $\psi_{osm} = const$, $\tau_{osm} = const$. The more comprehensive model of the osmotic growth of droplet should necessarily

Preprints (www.preprints.org) | NOT PEER-REVIEWED | Posted: 10 May 2021 doi:10.20944/preprints202105.0159.v1

consider a true non-perfectly-spherical shape of droplet and inevitably uneven distribution of salt over the droplet volume.

The "long-time" non-linear osmotic growth of droplets may be described by phenomenological Eq. 5, suggested recently in ref. 13.

$$\bar{R}(\bar{t}) = \sqrt[4]{\alpha - \beta exp(-\gamma \bar{t})}\,, \qquad (5)$$

where the triad α, β, and γ were taken as parameters (it is easily seen that the double Taylor expansion of Eq. 5 for $\bar{t} \to 0$ yields Eq. 4). The best possible fitting established with least square method, depicted with **Figure 8,** was obtained at $\alpha = 7.23$, $\beta = 6.22$, and $\gamma = 0.71$, which is in the semi-quantitative correspondence with Eq. 5.

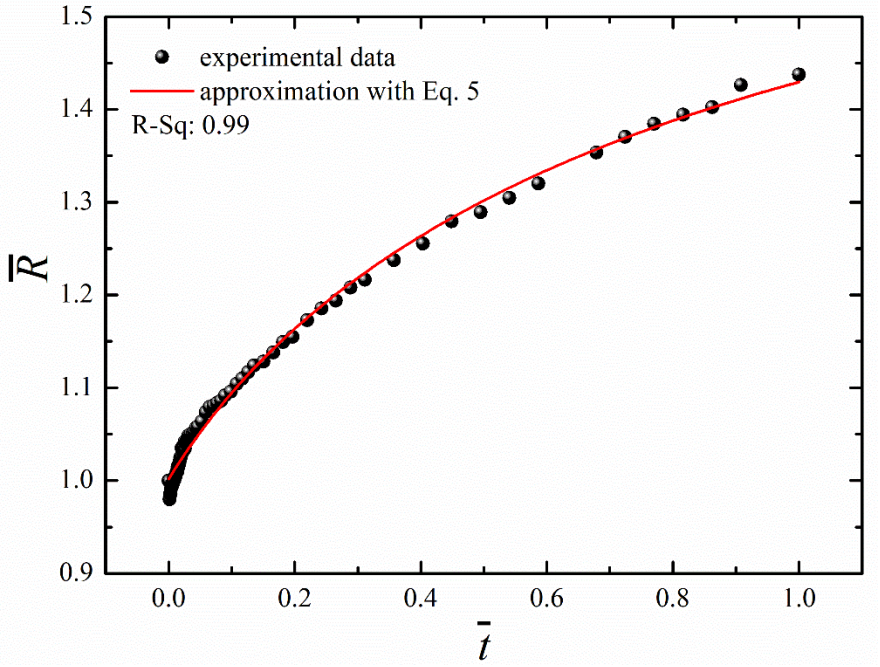

Figure 8. Time evolution of the dimensionless radius of the droplet (black circles) and its fitting with Eq. 5. $\bar{R} = \frac{R}{R_0}$ and $\bar{t} = \frac{t}{\tau_{osm}}$, where R_0 = 1.2 mm and $\tau_{osm} = 4875\ s$. The best possible fitting established with least square method, shown with a red solid line was established for $\alpha = 7.23, \beta = 6.22$ and $\gamma = 0.71$.

4. Conclusions

We conclude that water diffusion across thin floating PDMS film gives rise to the osmotic growth of the saline droplet placed on the film. The phenomenological model of the osmotic mass transfer is introduced. The model coincides satisfactorily with the observed experimental data. The osmotic growth of the droplet followed by evaporation of the droplet yields reversible growth/retraction cycles. The reversibility of the reported growth/retraction cycles should be emphasized. The reported PDMS

 doi:10.20944/preprints202105.0159.v1

membranes and process are of a potential for desalination and development of separators for batteries [27].

Funding

This research received no external funding.

Institutional Review Board Statement

Not applicable.

Informed Consent Statement

Not applicable.

Data Availability Statement

The data presented in this study are available on request from the corresponding author.

Author Contributions

Conceptualization, P.K.R., S. S. and E. B.; Methodology, P. K. R; L.D.; Software, P. K. R.; Validation, P. K. R. and E, B.; Formal Analysis, L. D.; Investigation, P.K. R., S.S., E.B. and L. D. ; Resources, S. S.; Data Curation, P. K, R.; Writing – Original Draft Preparation, E. B.; Writing – Review & Editing, S. S., E. B. and L. D.; Visualization, P. K. R.; Supervision, S. S. and E. B.; Project Administration, S. S.

Conflict of Interests

The authors declare no conflict of interests.

References

1. Mitrovski, S. M.; Elliott, L. C. C.; Nuzzo, R. G. Microfluidic devices for energy conversion: Planar integration and performance of a passive, fully immersed H_2–O_2 fuel cell. *Langmuir* **2004**, 20, 6974–6976.
2. Vankelecom, I. F. J.; De Kinderen, J.; Dewitte, B. M.; Uytterhoeven, J. B. Incorporation of hydrophobic porous fillers in PDMS membranes for use in pervaporation. *J. Phys. Chem.* **1997**, 101, 5182–5185.

3. Li, L.; Xiao, Z.; Tan, S.; Pu, L.; Zhang, Z. Composite PDMS membrane with high flux for the separation of organics from water by pervaporation. *J. Membr. Sci.* **2004**, 243, 177–187.

4. Fu, Y.-J.; Qui, H.-Z.; Liao, K.-S.; Lue, S. J.; Hu, C.-C.; Lee, K.-R.; Lai, J.-Y. Effect of UV-ozone treatment on poly(dimethylsiloxane) membranes: surface characterization and gas separation performance. *Langmuir* **2010**, 26, 4392–4399.

5. Firpo, G.; Angeli, E.; Repetto, L.; Valbusa, U. Permeability thickness dependence of polydimethylsiloxane (PDMS) membranes. *J. Membr. Sci.* **2015**, 481, 1–8.

6. Nour, M.; Berean, K.; Balendhran, S.; Ou, J. Z.; Du Plessis, J.; McSweeney, C.; Bhaskaran, M.; Sriram, S.; Kalantar-zadeh, K. CNT/PDMS composite membranes for H_2 and CH_4 gas separation. *Int. J. Hydrog. Energy* **2013**, 38, 10494–10501.

7. Nour, M.; Berean, K.; Griffin, M. J.; Matthews, G. I.; Bhaskaran, M.; Sriram, S.; Kalantar-zadeh, K. (2012). Nanocomposite carbon-PDMS membranes for gas separation. *Sens. Actuator B: Chem.* **2012**, 161, 982–988.

8. Sanchis-Perucho, P.; Robles, Á.; Durán, F.; Ferrer, J.; Seco, A. PDMS membranes for feasible recovery of dissolved methane from AnMBR effluents. *J. Membr. Sci.* **2020**, 604, 118070.

9. Ataeivarjovi, E.; Tang, Z.; Chen, J. Study on CO_2 Desorption Behavior of a PDMS–SiO_2 Hybrid Membrane Applied in a Novel CO_2 Capture Process. *ACS Appl. Mater. Interfaces* **2018**, 10, 28992–29002.

10. Logemann, M.; Alders, M.; Wist, M.; Pyankova, V.; Krakau, D.; Gottschalk, D.; Wessling, M. Can PDMS membranes separate aldehydes and alkenes at high temperatures? *J. Membr. Sci.* **2020**, 615, 118334.

11. Zheng, B.; Tice, J. D.; Roach, L. S.; Ismagilov, R. F. A droplet-based, composite PDMS/glass capillary microfluidic system for evaluating protein crystallization conditions by microbatch and vapor-diffusion methods with on-chip X-ray diffraction. *Angew. Chem. Int.* **2004**, 43, 2508–2511.

12. Zheng, B.; Gerdts, C. J.; Ismagilov, R. F. Using nanoliter plugs in microfluidics to facilitate and understand protein crystallization. *Curr. Opin. Struct. Biol.* **2005**, 15, 548–555.

13. Roy, P. K.; Legchenkova, I.; Shoval, S.; Dombrovsky, L. A.; Bormashenko, E. Osmotic evolution of composite liquid marbles. *J. Colloid Interface Sci.* **2021**, 592, 167–173.

14. Thangawng, A. L.; Ruoff, R. S.; Swartz, M. A.; Glucksberg, M. R. An ultra-thin PDMS membrane as a bio/micro–nano interface: fabrication and characterization. *Biomed Microdevices* **2007**, 9, 587–595.

15. Koo, J. W.; Ho, J. S.; An, J.; Zhang, Y.; Chua, C. K.; Chong, T. H. A review on spacers and membranes: Conventional or hybrid additive manufacturing? *Water Res.* **2020**, 188, 116497.

16. Zhang, R.; Liao, W.; Wang, Y.; Wang, Y.; Wilson, D. I.; Clarke, S. M.; Yang, Z. The growth and shrinkage of water droplets at the oil-solid interface. *J. Colloid & Interface Sci*. **2021**, *584*, 738-748.

17. Erbil H. Y. Surface Chemistry of Solid and Liquid Interfaces, Blackwell, Oxford, 2006.

18. Tadmor, R. Line energy and the relation between advancing, receding, and young contact angles. *Langmuir* **2004**, 20 (18), 7659–7664.

19. Tadmor, R. Approaches in wetting phenomena, *Soft Matter* **2011**, 7, 1577–1580.

20. Tadmor, R.; Yadav, P. S. As-placed contact angles for sessile drops. *J. Colloid Interface Sci.* **2008**, 317, 241–246.

21. Liu, J.; Xia, R.; Zhou, X. A new look on wetting models: continuum analysis. *Sci. China Phys. Mech. Astron.* **2012**, 55, 2158–2166.

22. Liu, J.; Mei, Y.; Xia, R. A new wetting mechanism based upon triple contact line pinning. *Langmuir* **2011**, 27, 196–200.

23. Bormashenko E.; Physics of Wetting Phenomena and Applications of Fluids on Surfaces, *de Gruyter*, **2017** Berlin.

24. Deegan, R. D.; Bakajin, O.; Dupont, T. F.; Huber, G.; Nagel, S. R.; Witten, T. A. Capillary flow as the cause of ring stains from dried liquid drops. *Nature* **1997**, 389, 827–829.

25. Deegan, R. D.; Bakajin, O.; Dupont, T. F.; Huber, G.; Nagel, S. R.; Witten, T. A. Contact line deposits in an evaporating drop, *Phys. Rev. E* **2000**, 62, 756–765.

26. Hu, H.; Larson, R. G. Analysis of the effects of Marangoni stresses on the microflow in an evaporating sessile droplet. *Langmuir* **2005**, 21, 3972–3980.

27. Angulakshmi, N.; Stephan, A. M. Efficient electrolytes for lithium–sulfur batteries. *Front. Energy Res*. **2015**, 3 (17), 1-8.

Preprints (www.preprints.org) | NOT PEER-REVIEWED | Posted: 10 May 2021 doi:10.20944/preprints202105.0159.v1

TOC Graphics